Published in IET Microwaves, Antennas & Propagation
Received on 15th January 2012
doi: 10.1049/iet-map.2012.0306

ISSN 1751-8725

Efficient ultrawideband propagation modelling by using the cubic B-spline function in ray tracing calculations

V. Mohtashami A.A. Shishegar

Department of Electrical Engineering, Sharif University of Technology, Tehran, Iran
E-mail: mohtashami@ee.sharif.edu

Abstract: In site-specific ultrawideband propagation modelling, electromagnetic field calculations need to be performed by ray tracing at numerous frequencies of the band in order to properly include the frequency variations of the propagation mechanisms and antenna patterns. This is computationally intensive especially in calculating the coverage map or finding the statistics of the channel parameters where field calculations need to be carried out at a lot of receiver locations. In this study, the cubic B-spline function is incorporated in ray tracing to increase the computational efficiency of site-specific ultrawideband propagation modelling. This function can accurately reconstruct a signal from a few samples at a low-computational cost. By calculating the electromagnetic fields at a few frequency samples followed by cubic B-spline reconstruction, a lot of unnecessary calculations of the post-processing stage are suppressed without degrading the accuracy of the results. The study develops a systematic procedure for determining the number of required frequency samples according to the geometrical and electromagnetic properties of the walls, frequency variations of the antenna patterns and characteristics of the cubic B-spline function. The proper functionality of the proposed method is verified by numerical results where the simulation time is reduced several times for a typical indoor environment.

1 Introduction

The ever-increasing demand for very high-speed indoor wireless communication can be well supplied by transmitting the data through ultrawideband (UWB) channels [1–4]. Typically, several gigahertz of bandwidth is available in ultrawideband communications as in UWB or 60 GHz bands. This leads to considerable frequency variation of the propagation mechanisms and the antenna patterns, which if neglected in system design, may degrade the quality of service. Hence, UWB propagation modelling involves more complicated effects compared with conventional narrowband or wideband channels.

There exist two completely different ways of UWB propagation modelling. Empirical methods based on extensive measurements inside buildings [5–8] and site-specific methods usually based on ray tracing simulations [9–13]. The outputs of the empirical methods are channel models based on the measurement results of real-world scenarios. However, these methods have several disadvantages. They do not provide a good physical insight to the propagation mechanisms. They require cumbersome data processing to extract the multipath components from the received signal. Measurement errors are almost always present which impact the derived channel model. The empirical methods are also very time consuming and costly. In contrast, ray tracing eliminates the aforementioned drawbacks to a great extent. It takes the plan of the building into account and provides a 'site-specific' model. The frequency dependence of the propagation mechanisms and antenna patterns can be analytically considered in ray tracing to predict the dispersion properties of the received signal. Therefore ray tracing is a more versatile method of UWB propagation modelling.

Ray tracing simulation of an UWB channel consists of two stages: a geometrical stage that traces the electromagnetic energy tubes out of the transmitter and a post-processing stage that computes the electromagnetic fields at the receiver locations. The geometrical stage is performed once and there exist numerous published articles on reducing its computational burden [14–16]. In the post-processing stage, however, field calculations need to be repeated for every receiving location. Therefore it is crucial to perform the calculations in a computationally efficient manner. In some research activities time domain formulations have been presented [17–22]. They assume closed-form models for frequency variations of the dielectric constants of materials and derive the time domain reflection, transmission and diffraction coefficients. However, these formulations are approximate and usually involve a series of Bessel functions which may be computationally intensive to calculate. Besides, the actual material properties (which are determined by measurements) may not follow the assumed dielectric constant models. These drawbacks motivate us to resort to frequency domain formulations, that is, repeating the conventional field calculations of ray tracing at several frequencies of the band. The formulations are very simple and also allow arbitrary frequency dependence of the dielectric constants. However, the

number of frequency samples at which the field calculations are performed must be large enough to include the effects of multipath components that have late times of arrival but still carry a considerable amount of energy. This imposes a heavy computational burden in applications where the number of receiving locations have to be large; for example, in calculating the coverage map or analysis of channel parameter statistics. To the best of the authors' knowledge, there exist few research activities with focus on reducing the computational complexity of post-processing. The authors of [9, 10] use parallel ray approximation to estimate the fields in the vicinity of a given receiver location. With proper phase correction and through the analysis of an appropriate error function, the coverage map was obtained by calculating the fields at relatively few receiver locations. Diskin and Brennan in [11] state that the field at the receiver is computed at a few frequency samples and the results are interpolated using a tenth degree polynomial by minimising the mean square error. The idea is brilliant but the method neglects transmission through the walls and more importantly multiple reflections inside the walls that cause the total reflection and transmission coefficients to vary much faster with frequency.

The original contribution of this paper is the utilisation of the cubic B-spline function in ray tracing for efficient calculation of the UWB channel's frequency response. The cubic B-spline function is a polynomial of the third degree with finite support. It has high accuracy and involves low-computational complexity in reconstructing a finitely supported signal from a few samples. In our approach, the shooting and bouncing ray (SBR) method is first used to determine the geometrical propagation paths of the electromagnetic energy tubes in the environment. Then, the post-processing stage is performed to calculate the electromagnetic fields at the receiver locations. In this stage, for a given receiver location, the frequency response of each arriving ray is calculated at a few frequency samples. Then, the cubic B-spline function is used to reconstruct the frequency response of that ray in the whole bandwidth of the channel. The number of required frequency samples are systematically determined from the frequency variations of the reflection, transmission and diffraction coefficients, frequency variations of the antenna patterns and the characteristics of the cubic B-spline function. By calculating the fields at a few frequencies and applying the accurate and computationally efficient cubic B-spline reconstruction, a significant saving in the simulation time of the post-processing stage can be achieved. An important point here is that the B-spline functions can be included in the wavelet category [23]. The wavelets have been used in electromagnetic simulations to reduce the computational burden of the numerical methods such as finite difference time domain (FDTD) and method of moments [24, 25]. However, the idea of using the cubic B-spline function in ray tracing for efficient calculation of the electromagnetic fields is novel and has not been presented yet.

The rest of the paper is organised as follows. Section 2 examines the frequency response of the UWB channel in detail. Section 3 discusses the reconstruction of a finitely supported signal from its samples and introduces the cubic B-spline function for this purpose. Section 4 provides a systematic procedure for reconstructing the frequency response of the UWB channel by using the cubic B-spline function. It also determines the number of required frequency samples. Section 5 presents some numerical results which show the computational efficiency enhancement of the post-processing stage. Section 6 concludes the paper.

2 Problem definition

The effect of an indoor environment on the UWB electromagnetic wave is best described by the channel's frequency response. Almost all descriptive channel parameters can be extracted from the frequency response or its inverse Fourier transform, the impulse response. Therefore accurate calculation of frequency response is of utmost importance.

At each receiving point the frequency response, denoted by $H(f)$, is the sum of the contributions of multipath rays whose wavefronts illuminate the receiver; that is

$$H(f) = \sum_{n=1}^{N} H_n(f) \tag{1}$$

where $H_n(f)$ is the frequency response of the nth multipath ray and N denotes the total number of rays arriving at the receiver. $H_n(f)$ can be written as

$$H_n(f) = (a_n(f)\mathrm{e}^{\mathrm{j}\phi_n(f)})\mathrm{e}^{-\mathrm{j}2\pi f\tau_n} \tag{2}$$

where τ_n is the propagation delay of the nth ray with respect to the first arriving ray. The term $a_n(f)\mathrm{e}^{\mathrm{j}\phi_n(f)}$ includes the effects of the radiation patterns of the transmitting and receiving antennas, the reflection and/or transmission coefficients of the walls encountered by the ray and the diffraction coefficients of the wedges hit by the ray. The effect of material dispersion on waves penetrating through the walls or on multiple reflections inside the walls is included in $a_n(f)\mathrm{e}^{\mathrm{j}\phi_n(f)}$ by using slab reflection and transmission coefficients. Usually, the frequency variation of $a_n(f)\mathrm{e}^{\mathrm{j}\phi_n(f)}$ is much slower than the propagation phase factor $\mathrm{e}^{-\mathrm{j}2\pi f\tau_n}$. This means that the frequency response $H(f)$ is accurately characterised if it is calculated at frequency samples spaced at most $\Delta f = 1/\max\{\tau_n\}_{n=1}^{N}$. Note that the propagation delays of all multipath rays are available from the geometrical stage of ray tracing and therefore the propagation phase factors are analytically known. The unknown part in each $H_n(f)$ is $a_n(f)\mathrm{e}^{\mathrm{j}\phi_n(f)}$ which has to be determined by calculating the antenna patterns and the reflection, transmission and diffraction coefficients at frequency samples separated $1/\max\{\tau_n\}_{n=1}^{N}$ from each other. These calculations dominate the runtime of post-processing which if reduced, will result in runtime saving being achieved. As mentioned, the frequency variation of $a_n(f)\mathrm{e}^{\mathrm{j}\phi_n(f)}$ is slow and will be fully considered even if $a_n(f)\mathrm{e}^{\mathrm{j}\phi_n(f)}$ is sampled at a frequency spacing much larger than $1/\max\{\tau_n\}_{n=1}^{N}$. A proper reconstruction (interpolation) method will afterwards reproduce $a_n(f)\mathrm{e}^{\mathrm{j}\phi_n(f)}$ at frequency samples spaced $1/\max\{\tau_n\}_{n=1}^{N}$ apart. In this way, a lot of unnecessary field calculations are avoided and simulation time reduction is achieved. The key part of this strategy is to use an accurate and low-complexity reconstruction method. The B-spline functions are suggested for this purpose and are described in the next section.

3 B-spline reconstruction of a sampled signal

3.1 Sampling and reconstruction of signals of finite support

From a mathematical point of view, polynomial interpolation is a good candidate for signal reconstruction. An nth degree

doi: 10.1049/iet-map.2012.0306

polynomial potentially has $n-1$ extrema and therefore for a large enough degree it is able to follow the original signal behaviour between the samples. This property, however, may also be regarded as a drawback when interpolating low-varying signals. In such a case, the interpolator tends to wiggle [26], a behaviour that is absent in the original signal. Furthermore, polynomial interpolation is not a 'local' procedure; that is if the original signal varies rapidly in some parts, its effect on the interpolator will be felt everywhere – even in those parts where the original signal varies smoothly. Classical Runge problem [27] is also an obstacle and may cause the polynomial interpolator not to converge to the original signal. Other versions of polynomial interpolation such as rational interpolation (including the well-known multipoint Padé approximation) possess singularity and unattainability problems in addition to the mentioned drawbacks [27].

From a signal processing point of view, however, the original signal can be investigated in a much better way and more sophisticated reconstruction methods can be utilised. Suppose that $f(x)$ is an arbitrary signal whose Fourier transform is $F(\omega)$. According to the sampling theorem, if $|F(\omega)| = 0$ for $|\omega| > \omega_M$, the original signal can be exactly reconstructed from its samples provided that the sampling frequency ω_s is at least twice ω_M. In the $\omega_s = 2\omega_M$ case (Nyquist rate), which results in the least number of samples and hence is called ideal sampling, the reconstructed signal $f_r(x)$ is derived from an infinite summation of the samples $\{f(mT)\}$ as [28]

$$f_r(x) = \sum_{m=-\infty}^{+\infty} f(mT)\, h(x - mT) \tag{3}$$

where $T = 2\pi/\omega_s$ is the sampling period and $h(x) = \mathrm{sinc}(x/T)$ is the impulse response of the ideal reconstruction filter. The associated frequency response of the filter is constant in $|\omega| < \omega_M$ and zero elsewhere.

If, however, $|F(\omega)|$ is not exactly zero for $|\omega| > \omega_M$, the reconstructed signal will not necessarily equal the original signal. This is true even if $|F(\omega)|$ has very small values in $|\omega| > \omega_M$. To get a better insight, consider the function $f(x) = e^{-x}(u(x) - u(x-10))$, where $u(x)$ is the unit step function. The magnitude of the Fourier transform of this function is non-zero for every ω but decays relatively sharply as $|\omega|$ increases. One may choose a large value as ω_M to ensure sufficient decay in $|F(\omega)|$, and then sample the signal with the Nyquist rate. Fig. 1 shows the reconstructed signal by applying this approach for three typical values of ω_M. At $\omega_M = 2\pi \times 5$, $|F(\omega)|$ decays 30 dB with respect to the maximum value of $|F(\omega)|$. This decay is 36 dB at $\omega_M = 2\pi \times 10$ and 44 dB at $\omega_M = 2\pi \times 25$. In all these cases $|F(\omega)|$ has negligible values in $|\omega| > \omega_M$. As observed, however, the reconstructed signal contains oscillations around the original signal no matter how large ω_M is considered. This phenomenon is referred to as ringing [28] and will be always present if $|F(\omega)|$ is not finitely supported. Hence, signals of finite support in the signal domain (which consequently have infinite support in the Fourier domain) will suffer from the ringing phenomenon as long as the ideal reconstruction filter is used. When modelling a UWB channel, the goal is to reconstruct the objective function $f(x) = a_n(x)e^{j\Phi_n(x)}$ from a few samples for every arriving ray, where x denotes the frequency, for example, 3.1 GHz $< x <$ 10.6 GHz for the UWB band. Thus, the objective function is of finite support and ideal reconstruction lacks sufficient accuracy.

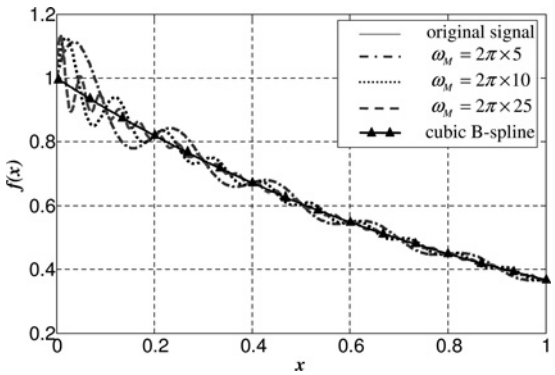

Fig. 1 *Reconstruction of the samples of $f(x) = e^{-x}(u(x) - u(x-10))$ with ideal filter and the cubic B-spline filter*

The ringing phenomenon is due to the 'sinc' shape of the impulse response of the reconstruction filter. The sinc function has infinite signal-domain support, behaves oscillatory, and has a low-decaying rate. In other words, ideal reconstruction is not a local procedure and the sinc function behaves like an infinite degree polynomial. A good option for reconstructing signals of finite support is to use a reconstruction filter whose impulse response has a finite support, least possible oscillation and a high-decaying rate. Such a reconstruction filter will have a frequency response of infinite support. However, if the frequency response of the filter has nearly constant gain in the pass band ($|\omega| < \omega_M$) and negligible values in the stop band ($|\omega - m\omega_s| < \omega_M$, $m = \pm1, \pm2, \ldots$), the reconstruction will be almost perfect. B-splines are mathematical functions that possess such properties as reconstruction filters. These properties will be highlighted in the following subsection.

3.2 B-splines as reconstruction filters

B-spline of nth order ($n = 0, 1, 2, \ldots$) is a piecewise polynomial function of degree n defined as [29]

$$\beta_n(x) = \frac{1}{n!}\sum_{k=0}^{n+1}(-1)^k \frac{(n+1)!}{k!(n-k+1)!} \times \left(x - k + \frac{n+1}{2}\right)^n u\left(x - k + \frac{n+1}{2}\right) \tag{4}$$

where $u(x)$ is the unit step function. B-spline of order n is of finite support and has non-zero value in $|x| < (n+1)/2$. For $n \geq 1$, it is continuous throughout $-\infty < x < +\infty$ along with its $n-1$ consecutive derivatives. B-splines of orders 0–5 are depicted in Fig. 2*a*.

B-spline of an arbitrary order can be used as a reconstruction filter. In that case, the reconstructed signal is expressed in terms of a weighted summation of shifted versions of the B-spline as

$$f_r(x) = \sum_{m=-\infty}^{+\infty} c_n(m)\beta_n\left(\frac{x - mT}{T}\right) \tag{5}$$

where T is the sampling period. The effort to find $\{c_n(m)\}$ leads to frequency response of the nth order B-spline

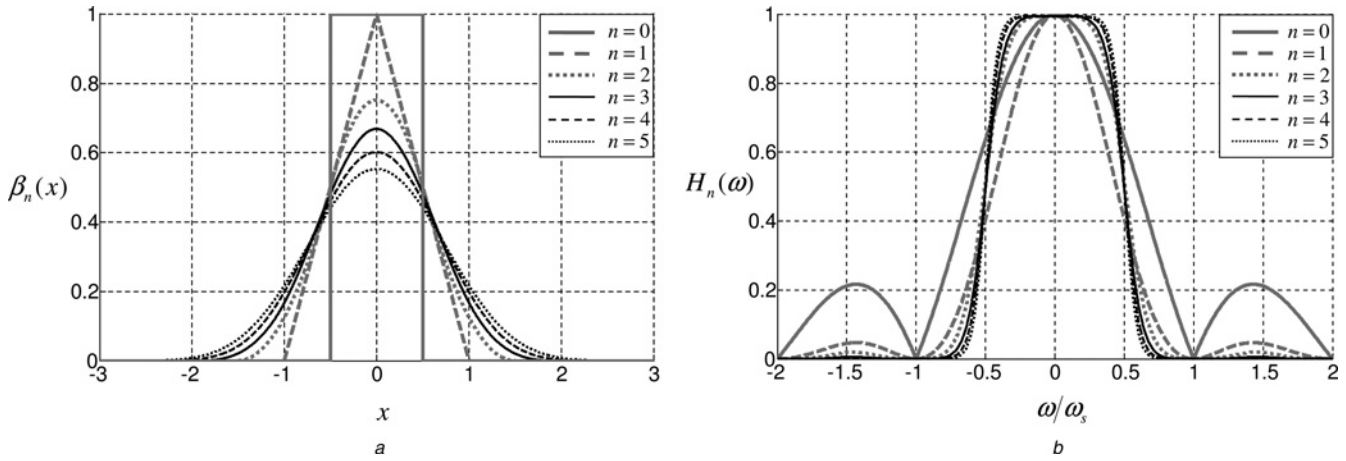

Fig. 2 *B-splines as reconstruction filters*

a *B*-spline functions
b Associated frequency responses of B-splines when used as reconstruction filters

reconstruction filter, $H_n(\omega)$, as

$$H_n(\omega) = \frac{\text{sinc}^{n+1}(\omega/\omega_s)}{\beta_n(0) + 2\sum_{k=1}^{\lfloor n/2 \rfloor} \beta_n(k)\cos(2\pi k(\omega/\omega_s))} \quad (6)$$

where operator $\lfloor\rfloor$ denotes the largest integer value not greater than its argument. Fig. 2*b* shows $H_n(\omega)$ for $n = 0, 1, \ldots, 5$. As observed, the increase in the order of B-spline results in more flatness of the frequency response in the pass band and smaller values in the stop band; a desirable property. As n increases, however, the support of $\beta_n(x)$ increases and its decaying rate decreases. This makes the reconstruction less local and consequently leads to more ringing in the reconstructed signal. Hence, there exists a trade-off for choosing the order of the B-spline.

Among various orders of the B-splines, the cubic B-spline ($n = 3$) encompasses the following interesting features that make it the suitable choice for signal reconstruction:

- The cubic B-spline is the lowest-order member of the B-spline family which has inflection point. The presence of the inflection point significantly smooths the reconstructed signal.
- In the variational calculus, it is shown that the cubic B-spline has minimum curvature among all functions that reconstruct a signal from the given data points [26]. Note that the presence of the ringing effect in a reconstructed signal increases its total curvature. Thus, the cubic B-spline reconstructs the smoothest function with least ringing.
- In order to find $\{c_n(m)\}$ in (5) and obtain the reconstructed signal, a linear equation system has to be solved whose coefficient matrix is tridiagonal and strictly row diagonally dominant [27]. Therefore the utilisation of the Gaussian elimination method for solving the equation system is possible which involves extremely low-computational complexity.

Referring to Fig. 2*b*, it is observed that by selecting $\omega_M = \omega_s/4$ (sampling with twice the Nyquist rate), the frequency response of the cubic B-spline will have constant gain in the pass band and at least 40 dB loss in the stop band. This results in accurate signal reconstruction and elimination of ringing. As illustrated in Fig. 1, the original signal is perfectly reconstructed by the cubic B-spline function from much fewer samples ($\omega_M = 2\pi \times 0.5$ at which $|F(\omega)|$ incurs only 10 dB loss) compared with ideal reconstruction.

The excellent characteristics of the cubic B-spline persuade us to use it for reconstructing the $a_n(f)e^{j\phi_n(f)}$ term in the wireless channel's frequency response. This will be discussed in a more detailed manner in the next section.

4 Cubic B-spline reconstruction of the frequency response of the UWB channel

Let $G_n(\nu)$ denote the Fourier transform of $g_n(f) = a_n(f)e^{j\phi_n(f)}$. By cubic B-spline reconstruction of the field data calculated at frequency samples spaced $\Delta f = 1/(4\nu_{\max})$ apart, $g_n(f)$ can be accurately obtained for all values of f. We mean by $\nu_{\max}$ the maximum value of ν after which $|G_n(\nu)|$ is 'effectively' zero. The objective of this section is to present a systematic way of determining $\nu_{\max}$ for each multipath component that arrives at the receiver. Since $g_n(f)$ is the resultant of consecutive propagation mechanisms (reflections, transmissions and diffractions) and antenna patterns, the Fourier analysis of these effects will lead us to the value of $\nu_{\max}$. It is very important to note that the analyses of the following subsections are performed prior to starting the post-processing stage. Hence, no extra computational burden is imposed on the post-processing stage. Rather, post-processing is provided with a guideline to select the necessary and sufficient number of frequency samples and avoid unnecessary calculations.

4.1 Reflection

Most indoor objects such as walls, doors and partitions are well modelled by dielectric slabs. The reflection coefficient of a ray impinging at an angle θ_i on a dielectric slab of thickness d and dielectric constant $\varepsilon_r = \varepsilon_r' - j\varepsilon_r''$ is [30]

$$\Gamma(f) = \frac{R(1 - e^{-2\gamma})}{1 - R^2 e^{-2\gamma}} \quad (7)$$

where $\gamma = jk_0 d(\varepsilon_r' - j\varepsilon_r'' - \sin^2\theta_i)^{1/2}$, k_0 is the free space propagation constant and R is the Fresnel reflection coefficient. This equation holds for both perpendicular and parallel polarisations provided that the corresponding Fresnel reflection coefficient is used. If the dielectric slab is

doi: 10.1049/iet-map.2012.0306

low loss (which is often true for indoor objects), the binomial expansion can be used to approximate $\gamma = \alpha + j\beta$ as

$$\alpha = \frac{k_0 d\varepsilon_r''}{2\sqrt{\varepsilon_r' - \sin^2\theta_i}} \tag{8}$$

$$\beta = k_0 d\sqrt{\varepsilon_r' - \sin^2\theta_i} \tag{9}$$

Obviously, α and β vary with frequency. Now, consider the conventional frequency variation model of the dielectric constant where ε_r' is frequency independent and ε_r'' is inversely proportional to the frequency; that is, $\varepsilon_r = \varepsilon_r' - j\sigma/(2\pi f\varepsilon_0)$ (σ is the conductivity of the material). The values of α and β will be, respectively, frequency independent and linear function of frequency. Let us rewrite (7) by using the geometrical series expansion of its denominator as

$$\begin{aligned}\Gamma(f) &= R(1 - \mathrm{e}^{-2\gamma})(1 + R^2\mathrm{e}^{-2\gamma} + R^4\mathrm{e}^{-4\gamma} + \cdots) \\ &= \sum_{m=0}^{\infty} a_m \mathrm{e}^{-\mathrm{j}2m\beta}\end{aligned} \tag{10}$$

where $a_0 = R$ and $a_m = (R - 1/R)R^{2m}\mathrm{e}^{-2m\alpha}$, $m \geq 1$. The low-loss assumption and frequency invariance of ε_r' leads to almost a frequency-independent value for R. As a result, the Fourier transform of $\Gamma(f)$, denoted by $\widetilde{\Gamma}(\nu)$, is

$$\widetilde{\Gamma}(\nu) = \sum_{m=0}^{\infty} a_m \delta\left(\nu - \frac{2m}{F}\right) \tag{11}$$

where F is called the 'fundamental period' which is a function of the incident angle and is equal to

$$F = \frac{c_0}{d\sqrt{\varepsilon_r' - \sin^2\theta_i}} \tag{12}$$

where c_0 is the speed of light in free space. Note that $\{a_m\}$ is a descending sequence and for a large enough M, the values of a_m, $m > M$, will have little effect on the value of $\Gamma(f)$. If we truncate the series representation of $\Gamma(f)$ at $m = M$, then $\nu_{\max} = 2M/F$. The sampling period of $\Gamma(f)$ for cubic B-spline reconstruction will therefore be $\Delta f = F/(8M)$. Hence, if the fundamental period F and the truncation order M are known, the reflection coefficient can be accurately reconstructed from samples spaced at $\Delta f = F/(8M)$.

The required frequency spacing based on the $\Delta f = F/(8M)$ formula is rather tricky in the sense that the truncation order M is itself a function of frequency. This means that the series representation of $\Gamma(f)$ may converge with different number of terms at different frequencies. To account for this, it is logical to consider the convergence of $\Gamma(f)$ in the whole bandwidth of the channel. Let us define the following error function for checking the convergence of $\Gamma(f)$ and finding the truncation order

$$e(f, \theta_i, m) = \left|1 - |\Gamma(f, \theta_i)|_m / |\Gamma(f, \theta_i)|_{m+1}\right| \tag{13}$$

where $|\Gamma(f, \theta_i)|_m$ means the magnitude of the reflection coefficient assuming that the truncation order is m. The value of this error function shows the contribution of a_{m+1} in the reflection coefficient at incident angle θ_i and frequency f. In order to consider the overall contribution of a_{m+1} in the reflection coefficient at incident angle θ_i, we may average the error function in the whole bandwidth of the channel $f_{\min} < f < f_{\max}$. This leads to the average error function $\overline{e}(\theta_i, m)$ as

$$\overline{e}(\theta_i, m) = \frac{1}{f_{\max} - f_{\min}} \int_{f_{\min}}^{f_{\max}} e(f, \theta_i, m)\,\mathrm{d}f \tag{14}$$

For each value of θ_i, there exists a value of truncation order M such that $\overline{e}(\theta_i, M) \geq \varepsilon$ and $\overline{e}(\theta_i, M + 1) < \varepsilon$ where ε is a predefined threshold close to zero. We denote this value of truncation order by $M(\theta_i)$ to emphasise its dependence on the incident angle. As a result, $\nu_{\max}(\theta_i) = 2M(\theta_i)/F(\theta_i)$ and $\Delta f(\theta_i) = F(\theta_i)/(8M(\theta_i))$. By following this procedure for each of the two polarisations (perpendicular, parallel), the associated $\Delta f(\theta_i)$ is found. The minimum of the two values at each θ_i is selected as the required frequency spacing and denoted by $\Delta f_{\mathrm{R}}(\theta_i)$. For a ray that impinges on the wall at incident angle θ_i, the post-processing stage reconstructs the reflection coefficient from samples spaced at $\Delta f_{\mathrm{R}}(\theta_i)$.

4.2 Transmission

The transmission coefficient of a ray incident on a dielectric slab is [30]

$$\tau(f) = \frac{(1 - R^2)\mathrm{e}^{-\gamma}}{1 - R^2\mathrm{e}^{-2\gamma}} = \sum_{m=0}^{\infty} a_m \mathrm{e}^{-\mathrm{j}(2m+1)\beta} \tag{15}$$

where $a_m = (1 - R^2)R^{2m}e^{-(2m+1)\alpha}$, $m \geq 0$. If the series is truncated at $m = M$, then $\nu_{\max} = (2M + 1)/F$. Following the same procedure as stated for the reflection case, we can determine $\nu_{\max}(\theta_i)$ for reconstruction of the transmission coefficient. To do this Γ is replaced with τ in (13) and the averaging over frequency is performed. Then $\nu_{\max}(\theta_i)$ or equivalently $\Delta f(\theta_i) = 1/(4\nu_{\max}(\theta_i))$ is obtained for the two polarisation types. The minimum of the two values of $\Delta f(\theta_i)$ at each incident angle is selected as the required frequency spacing for reconstruction of the transmission coefficient and is denoted by $\Delta f_{\mathrm{T}}(\theta_i)$.

4.3 Sequence of reflections and/or transmissions

A ray that arrives at the receiver may have encountered several reflections and/or transmissions. Therefore its electromagnetic field includes the multiplication of the reflection and/or transmission coefficients of the intersected walls. In this subsection, we wish to determine the frequency spacing that is required for cubic B-spline reconstruction of a multiplication of reflection and/or transmission coefficients.

Consider the consecutive reflections from two walls with reflection coefficients $\Gamma^{(1)}(f)$ and $\Gamma^{(2)}(f)$ and incident angles θ_{i_1} and θ_{i_2}. The total reflection coefficient is $\Gamma^{(\mathrm{total})}(f) = \Gamma^{(1)}(f)\,\Gamma^{(2)}(f)$. Consequently

$$\begin{aligned}\widetilde{\Gamma}^{(\mathrm{total})}(\nu) &= \widetilde{\Gamma}^{(1)}(\nu) * \widetilde{\Gamma}^{(2)}(\nu) \\ &= \sum_{m_1=0}^{M_1(\theta_{i_1})} \sum_{m_2=0}^{M_2(\theta_{i_2})} a_{m_1} a_{m_2} \delta\left(\nu - \frac{2m_1}{F_1(\theta_{i_1})} - \frac{2m_2}{F_2(\theta_{i_2})}\right)\end{aligned} \tag{16}$$

where $*$ denotes convolution, $F_1(\theta_{i_1})$, $F_2(\theta_{i_2})$ are the fundamental periods of the two walls and $M_1(\theta_{i_1})$, $M_2(\theta_{i_2})$ are the associated truncation orders of the two reflection coefficients which are chosen according to the procedure described in Section 4.1. The maximum available harmonic in $\Gamma^{(\text{total})}$ is

$$\begin{aligned}\nu_{\max}^{(\text{total})} &= 2M_1(\theta_{i_1})/F_1(\theta_{i_1}) + 2M_2(\theta_{i_2})/F_2(\theta_{i_2}) \\ &= \nu_{\max}^{(1)}(\theta_{i_1}) + \nu_{\max}^{(2)}(\theta_{i_2})\end{aligned}$$

Therefore

$$\frac{1}{\Delta f^{(\text{total})}} = \frac{1}{\Delta f_R^{(1)}(\theta_{i_1})} + \frac{1}{\Delta f_R^{(2)}(\theta_{i_2})} \tag{17}$$

In other words, if the geometrical stage of ray tracing finds that a ray has been consecutively reflected from two walls at incident angles θ_{i_1} and θ_{i_2}, then the post-processing stage needs to sample the total reflection coefficient at $\Delta f^{(\text{total})}$ calculated from (17). The proper performance of this procedure will be shown in Section 5.

The generalisation of the above result to K consecutive intersections leads to

$$\frac{1}{\Delta f^{(\text{total})}} = \sum_{k=1}^{K} \frac{1}{\Delta f_P^{(k)}(\theta_{i_k})} \tag{18}$$

where θ_{i_k} is the incident angle at kth intersection. The subscript P specifies the type of the propagation mechanism: $P = R$ when the kth intersection involves reflection and $P = T$ when the kth intersection involves transmission.

4.4 Extension to arbitrary frequency variation of the dielectric constants

So far, we have assumed that for each building material ε_r' is constant and ε_r'' is inversely proportional to frequency. The dielectric constants of indoor objects usually follow this model quite well. For more accurate indoor propagation modelling, however, it is better to measure the dielectric constants of the materials of the site and then use them in ray tracing [31, 32]. In that case, the real and imaginary parts of the dielectric constants may not exactly follow the aforementioned dielectric model though the low-loss property is usually maintained. Furthermore, β is no longer a linear function of frequency and the definition of the fundamental period in (12) is useless. Nevertheless, for most building materials, $\beta(f)$ negligibly deviates from linear dependence on frequency. It is therefore logical to perform a linear regression on the values of $\beta(f)$. The resulting fundamental period, denoted by $\overline{F}(\theta_i)$, is calculated via a least square algorithm which yields

$$\frac{1}{\overline{F}(\theta_i)} = \frac{1}{f_{\max} - f_{\min}} \int_{f_{\min}}^{f_{\max}} \frac{d}{c_0} \sqrt{\varepsilon_r'(f) - \sin^2\theta_i}\, df \tag{19}$$

Now, the procedure for determining $\nu_{\max}(\theta_i)$ and $\Delta f(\theta_i)$ as described before is performed by replacing $F(\theta_i)$ with $\overline{F}(\theta_i)$. In fact, (19) indicates a frequency averaging procedure to obtain an overall behaviour of the fundamental period. Hence, $\overline{F}(\theta_i)$ is called the average fundamental period. The proper performance of the average fundamental period is shown in Section 5.

4.5 Diffraction

In an indoor environment, diffraction from lossy dielectric wedges is well modelled by using Lubbers diffraction coefficient [33]. This diffraction coefficient is a function of the geometrical description of the wedge and TX–RX locations. The dependency of the diffraction coefficient on the wedge distances from TX and RX makes it difficult to find a function $\nu_{\max}(\theta_i)$ for its reconstruction prior to starting the post-processing stage. However, the diffraction coefficient follows $\hat{F}(f)/\sqrt{f}$ frequency dependence where $\hat{F}(.)$ is the Fresnel transition integral [34]. This function is depicted in Fig. 3*a* and, as observed, varies smoothly. The square root is also a smooth function of its argument. Consequently, as illustrated in Fig. 3*b*, the frequency variation of the diffraction coefficient is quite smooth. This means that the diffraction coefficient can be reconstructed from much fewer samples compared with resonant-looking frequency-dependent reflection and transmission coefficients. Therefore if a diffraction happens within a sequence of reflections and/or transmissions, the required frequency spacing between the samples for cubic B-spline reconstruction is still accurately calculated by (18). If a ray encounters only diffraction between TX and RX, the required frequency spacing is determined by the antenna patterns through the general formula (20) in Section 4.7.

4.6 Antenna pattern

To accurately reconstruct the frequency dependent antenna pattern, its Fourier transform is calculated at each angle of departure (θ, φ) and the corresponding $\nu_{\max}(\theta, \varphi)$ is

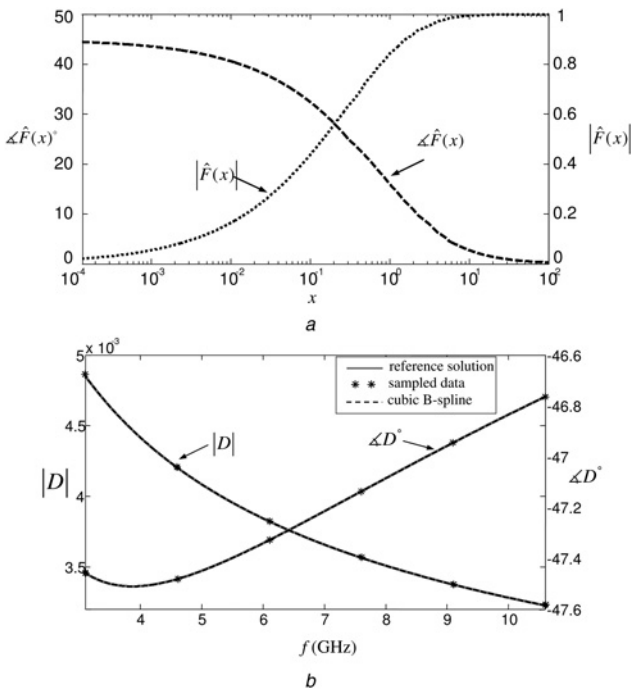

Fig. 3 *The cubic B-spline function for reconstruction of the diffraction coefficient*

a Fresnel transition integral

b Frequency variation of the magnitude and phase of the diffraction coefficient of a perpendicularly polarised ray impinging on right-angle brick wall. The permittivity of brick is taken from [31], $\theta_i = 10^\circ$, $\theta_d = 115^\circ$ and $\Delta f = 1500$ MHz is used as frequency spacing of the sampled data

doi: 10.1049/iet-map.2012.0306

obtained. By choosing $\Delta f(\theta,\ \varphi) = 1/(4\nu_{\max}(\theta,\ \varphi))$, the antenna pattern can be accurately reconstructed by the cubic B-spline function at the angle of departure/arrival (θ, φ).

4.7 Implementation in post-processing

Prior to starting the post-processing stage, $\Delta f_{\mathrm{R}}(\theta_i)$ and $\Delta f_{\mathrm{T}}(\theta_i)$ are calculated for each wall of the environment. The required frequency spacings to reconstruct the antenna patterns are also obtained. The low-varying part of the frequency response of the nth ray, that is, $g_n(f)$, includes the multiplication of the antenna patterns and the reflection/transmission/diffraction coefficients. According to the discussions presented in the previous subsections the required frequency spacing, $\Delta f^{(\mathrm{total})}$, for cubic B-spline reconstruction of $g_n(f)$ is calculated as

$$\frac{1}{\Delta f^{(\mathrm{total})}} = \frac{1}{\Delta f_{\mathrm{TX}}(\theta_{\mathrm{TX}}, \varphi_{\mathrm{TX}})} + \sum_{k=1}^{K} \frac{1}{\Delta f_P^{(k)}(\theta_{i_k})} + \frac{1}{\Delta f_{\mathrm{RX}}(\theta_{\mathrm{RX}}, \varphi_{\mathrm{RX}})} \tag{20}$$

where $(\theta_{\mathrm{TX}}, \varphi_{\mathrm{TX}})$ is the angle of departure from the transmitter, $(\theta_{\mathrm{RX}}, \varphi_{\mathrm{RX}})$ is the angle of arrival at the receiver, $\Delta f_{\mathrm{TX}}(\theta_{\mathrm{TX}}, \varphi_{\mathrm{TX}})$ and $\Delta f_{\mathrm{RX}}(\theta_{\mathrm{RX}}, \varphi_{\mathrm{RX}})$ are, respectively, the frequency spacings imposed by the transmitting and receiving antennas, K is the number of walls intersected by the ray and the definition of $\Delta f_P^{(k)}(\theta_{i_k})$ is the same as in (18). Therefore to obtain $g_n(f)$ the post-processing stage performs the electromagnetic field computations at frequency samples spaced $\Delta f^{(\mathrm{total})}$ apart. Then, the cubic B-spline reconstruction is used to reproduce $g_n(f)$ at frequency samples spaced $\Delta f = 1/\max\{\tau_n\}_{n=1}^{N}$ apart. $H_n(f)$ is obtained by multiplying $g_n(f)$ by the corresponding propagation phase factor. This procedure is repeated for all arriving rays to obtain the frequency response. As will be shortly observed, the presented method is very effective in reducing the simulation time of post-processing.

5 Numerical results

In this section the computational efficiency improvement offered by incorporating the cubic B-spline function in the post-processing stage is investigated. At first, we present a set of simple examples to validate the presented procedure for finding $\Delta f(\theta_i)$. Consider a 12 cm thick brick wall with $\varepsilon_r' = 4.75$ and $\sigma = 0.06$ S/m in the UWB frequency range $3.1 < f_{(\mathrm{GHz})} < 10.6$. The low-loss assumption holds in the whole bandwidth and the predefined threshold for determining the truncation order is selected $\varepsilon = 5\%$. The value of $\Delta f_R(\theta_i)$ is calculated for this wall according to the procedure described in Section 4.1 and is depicted in Fig. 4. For a ray that impinges on this wall at $\theta_i = 40^\circ$ we have $\Delta f_R = 150$ MHz. Fig. 5*a* shows the cubic B-spline reconstructed reflection coefficient from the sampled data spaced 150 MHz apart compared with the reference solution, that is, the reflection coefficient calculated with a very fine 1 MHz resolution. The incident angle is $\theta_i = 40^\circ$. Excellent agreement is observed which proves the proper functionality of the method.

For validating the procedure of obtaining $\Delta f_{\mathrm{T}}(\theta_i)$, a 4 cm thick wooden door with $\varepsilon_r' = 3$ and $\sigma = 0.005$ S/m in the UWB frequency range is simulated and Δf_{T} as a function of the incident angle is obtained. Now, consider a ray incident on this door at $\theta_i = 30^\circ$. For this ray $\Delta f_{\mathrm{T}}(\theta_i)$ is found to be 380 MHz. Fig. 5*b* compares the cubic B-spline reconstructed transmission coefficient of this ray (from samples spaced 380 MHz apart) with the reference solution (calculated with a 1 MHz resolution). As observed, the two curves have an excellent agreement with each other.

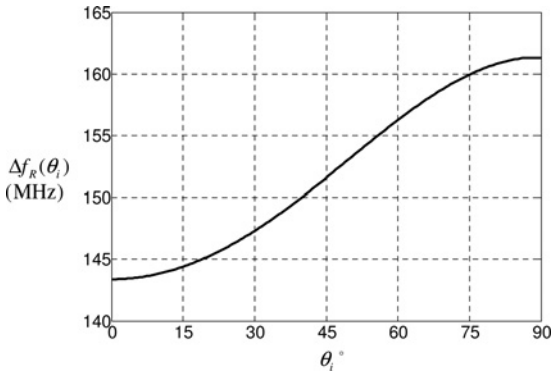

Fig. 4 *Required frequency spacing for cubic B-spline reconstruction of the reflection coefficient from a brick wall*

To validate (18) for consecutive intersections, the following simulation is considered. A ray with incident angle $\theta_i = 60^\circ$ is reflected from a concrete wall ($\varepsilon_r' = 7$, $\sigma = 0.03$ S/m, $d = 15$ cm, $\Delta f_{\mathrm{R}}(\theta_i) = 100$ MHz), then with an incident angle $\theta_i = 20^\circ$ is transmitted through a wooden door ($\varepsilon_r' = 3$, $\sigma = 0.005$, $d = 4$ cm, $\Delta f_{\mathrm{T}}(\theta_i) = 370$ MHz) and then with an incident angle $\theta_i = 30^\circ$ is reflected from a brick wall ($\varepsilon_r' = 4.75$, $\sigma = 0.06$ S/m, $d = 10$ cm, $\Delta f_{\mathrm{R}}(\theta_i) = 180$ MHz). The value of $\Delta f^{(\mathrm{total})}$ is calculated according to (18) which equals 54 MHz. Fig. 6*a* shows the cubic B-spline reconstructed coefficient compared with the reference solution. As observed, the reconstructed data matches the reference data very well.

The effective performance of the average fundamental period (obtained according to (19)) is verified in Fig. 6*b* where the reflection coefficient after two consecutive reflections from a 4 cm thick wooden door and a 10 cm thick brick wall is depicted. The frequency dependence of the dielectric constants is used according to [31] and the incident angles are 15° and 50°, respectively. As observed, the cubic B-spline reconstruction of the reflection coefficient yields accurate results.

The simple simulations presented above validate the excellent accuracy of the cubic B-spline function for reconstruction of the UWB electromagnetic fields from a limited set of samples. Now, we wish to investigate the computational efficiency enhancement that can be achieved when simulating a realistic indoor environment. Fig. 7 shows the plan of a two-room office environment. There are concrete ceiling and floor, brick walls, wooden doors, glass windows and some wooden cubicles in the building. The height of the ceiling is 3 m from the floor. The UWB frequency band is selected for the simulations. The electromagnetic properties of the building materials are chosen in accordance with the extensive measurements provided in [31]. The thicknesses of the building structures are provided in Table 1. For each wall type a pre-processing is performed to find Δf_{R} and Δf_{T} as functions of the incident angle. The average values of Δf_{R} and Δf_{T} are provided in Table 1 in order to give an insight on the typical values of the required frequency spacings. The computational cost of this pre-processing is absolutely negligible compared with those of the geometrical and post-processing stages.

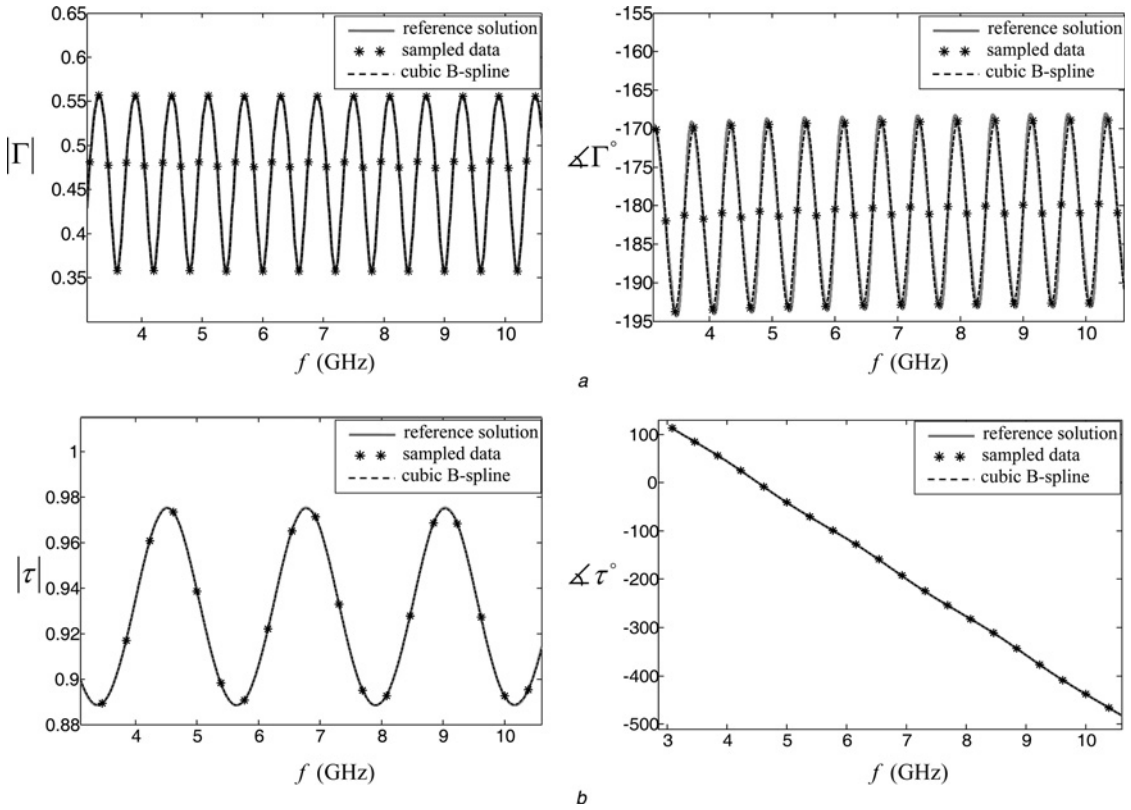

Fig. 5 *Magnitude and phase of the reflection/transmission coefficient reconstructed by the cubic B-spline function compared with the reference solution*

a Reflection from a brick wall in perpendicular polarisation
b Transmission through a wooden door in parallel polarisation

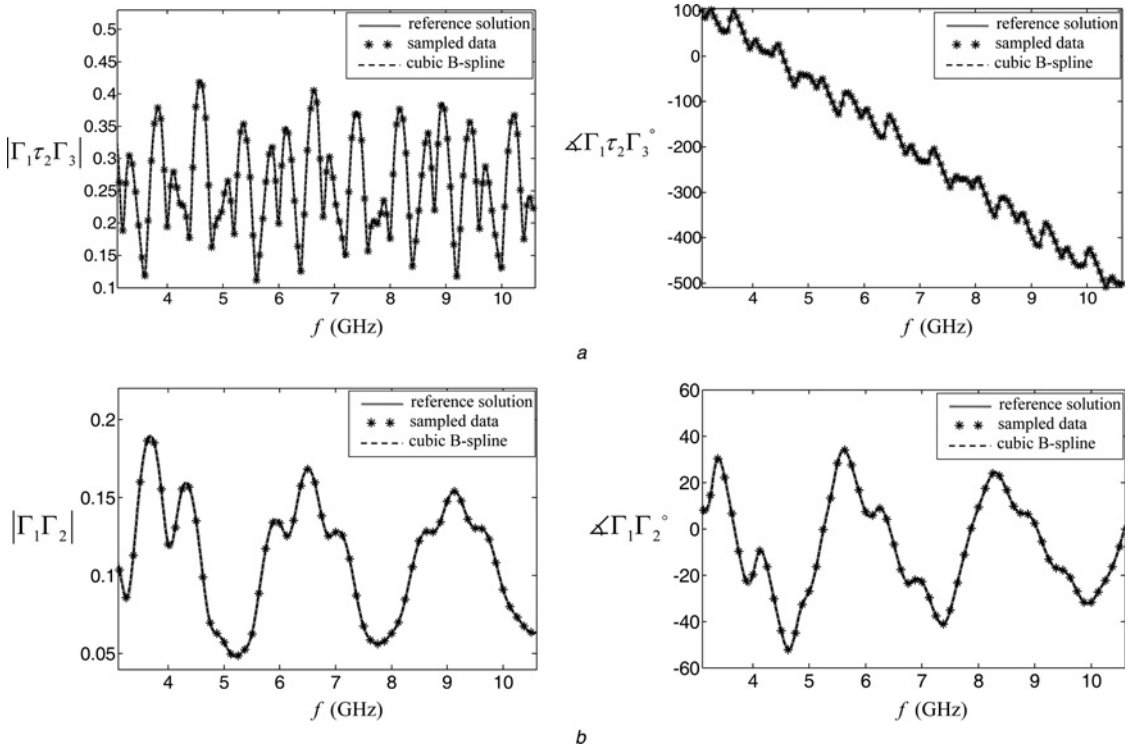

Fig. 6 *Cubic B-spline reconstruction of consecutive intersections*

a Simple dielectric constant model
b Dielectric constants according to the measured data in [31]

doi: 10.1049/iet-map.2012.0306

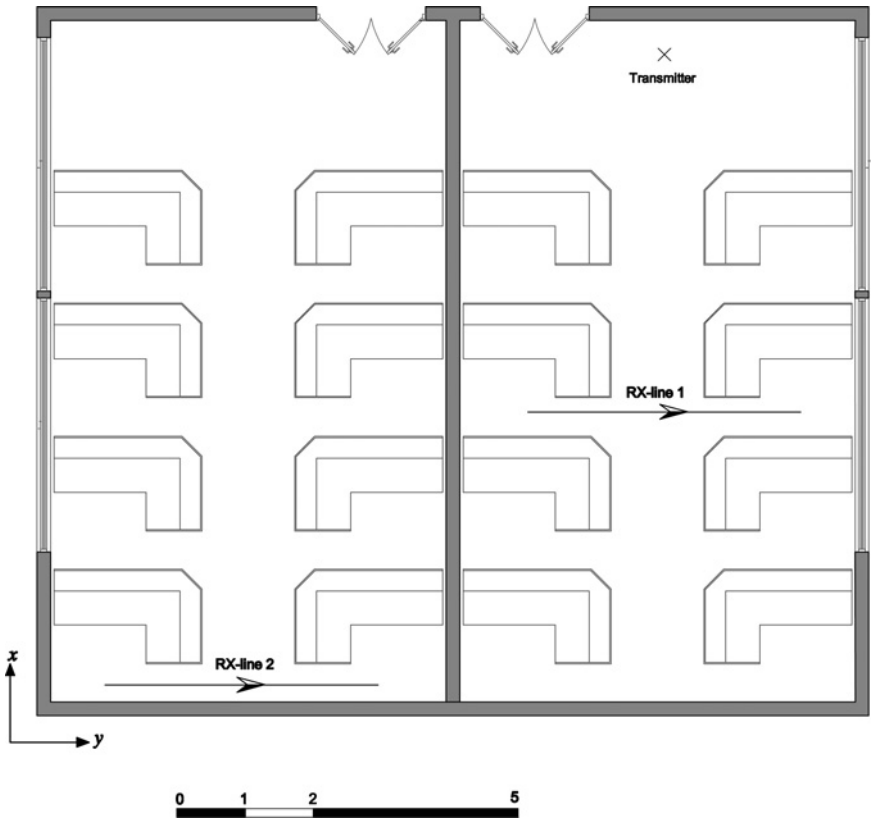

Fig. 7 *Plan of the simulated environment*

In the geometrical stage of ray tracing the propagation paths of the electromagnetic energy tubes are determined in the environment. The SBR method is used as the preferred ray tracing scheme because it provides good accuracy and also has less computational burden in indoor environments compared with the image method [35, 36]. The binary space partitioning acceleration technique [37] has been implemented in the SBR method to further reduce the simulation time of the geometrical stage. This ray tracing code has been prepared by the authors and its accuracy and proper functionality have been validated in [14]. To determine the propagation paths accurately, a high-resolution simulation is required. Thus, 100 002 rays have been launched from the transmitter and traced up to six bounces. This geometrical simulation takes 12 min and 36 s by using MATLAB software on a PC with a 2 GHz Intel Core 2 Duo processor and 2 GB of RAM.

The post-processing stage follows the geometrical stage using MATLAB on the same PC. At the transmitting and receiving ends, two vertically polarised wideband omnidirectional discone antennas are used. The associated frequency-dependent antenna pattern is included in post-processing according to the analytical formulations provided in [38]. The pattern varies very smoothly with frequency. This result in Δf_{TX} and Δf_{RX} range around 2000 MHz for different angles of departure/arrival. A total number of 400 points along two paths are considered as receiving locations. The TX and the RX points are located at heights of 2.5 m and 1.2 m from the floor, respectively. The heights of the cubicles are such that there is always an line-of-sight (LOS) propagation path between the TX and RX points along RX-line 1. Careful investigation of the UWB channel parameters shows that the considered six bounces ensure the convergence of the results. To explore the computational efficiency improvement, two different simulations are performed. In the reference simulation, the post-processing of the data is performed using the frequency step $\Delta f = 5$ MHz. Therefore multipath components with delays up to 200 ns are included which is observed to guarantee the arrival of all rays with considerable power in this environment. The typical number of multipath components that arrive at each RX point is 420 in the LOS path (RX-line 1) and 140 in the none-line-of-sight (NLOS) path (RX-line 2). Such large numbers of arriving multipaths are because of the presence of so many cubicles in the environment that generate various propagation paths. In the second simulation, the low-varying part of the frequency response of each arriving

Table 1 Characteristics of the building walls used in the simulation

Wall type	Material	Thickness, cm	Average Δf_R, MHz	Average Δf_T, MHz
ceiling and floor	concrete	25	1650	238
external and internal walls	brick	20	2250	189
doors	wood	4.5	656	1028
cubicles	wood	2	1261	1979
windows	glass	0.4	1659	1575

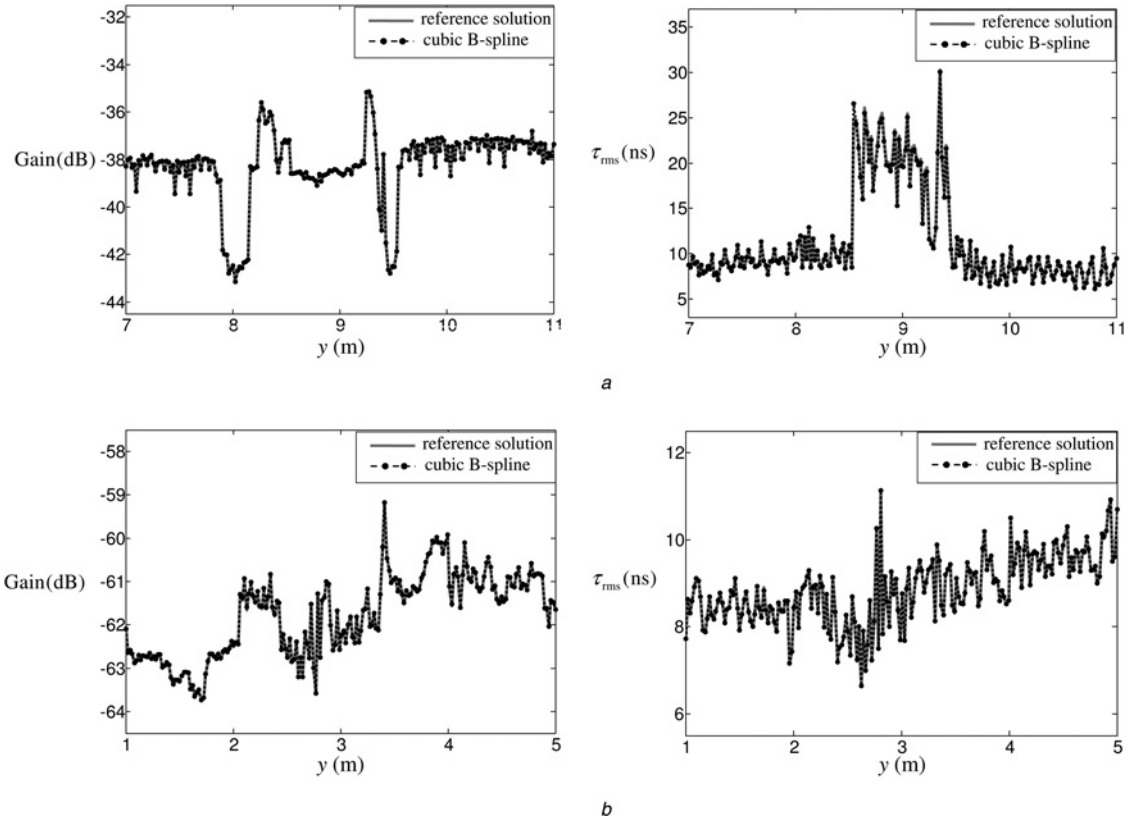

Fig. 8 *Path gain and rms delay spread calculated by cubic B-spline reconstruction compared with the reference solution*

a RX-line 1 (LOS path)
b RX-line 2 (NLOS path)

multipath component is computed at a much larger frequency step according to the formulations of Section 4 and the values of $\Delta f_R(\theta_i)$ and $\Delta f_T(\theta_i)$ obtained from pre-processing. The frequency responses are then reconstructed at $\Delta f = 5$ MHz by the cubic B-spline function followed by including the associated propagation phase factor. In both simulations, the path gain and rms delay spread at the receiving locations are calculated from the frequency responses. The results of the two simulations are compared in Fig. 8 and the simulation times are provided in Table 2. When the cubic B-spline function is used the post-processing is accelerated more than seven times in the LOS case and more than six times in the NLOS case. By including the simulation time of the geometrical stage the total simulation speedup is obtained and shown in Table 2. Still, a good simulation time improvement is achieved. Besides, in applications where the number of RX points has to be large the post-processing time becomes the dominant part of the total simulation time. In that case, the total simulation speedup increases and approaches the post-processing speedup. It is important to note that this acceleration is achieved without losing the accuracy of the results. As we can see in Fig. 8, the obtained curves are indistinguishable. In each graph, the mean relative error of the cubic B-spline result with respect to the reference solution (i.e.

$$\frac{1}{N}\sum_{n=1}^{N}\left|\frac{x_n^{(\mathrm{spl})}-x_n^{(\mathrm{ref})}}{x_n^{(\mathrm{ref})}}\right|$$

where $N = 200$ is the number of RX points, $x_n^{(\mathrm{spl})}$ and $x_n^{(\mathrm{ref})}$ are, respectively, the results of the cubic B-spline and reference solution at nth RX point) is provided in Table 2. This error is less than 1% in all cases and thus can be absolutely neglected in engineering applications. This means that the cubic B-spline function can be effectively used in post-processing to reduce the simulation time of the site-specific UWB propagation modelling. It is finally emphasised that the 'idea' of using the cubic B-spline function for accelerating post-processing is effective irrespective of the programming language used. The MATLAB software has been utilised in this research because of simple programming features and ease of implementation. More sophisticated programming languages can be alternatively used which may further enhance the simulation speedup.

So far, we have presented a systematic way of determining the number of frequency samples for cubic B-spline reconstruction of each ray's frequency response. It will be interesting to investigate the 'overall' number of required frequency samples and relate it to the site-specific nature of the environment. Fig. 9 shows the statistical distribution of

Table 2 Simulation results

Receiving path	RX-line 1	RX-line 2
number of receiving locations	200	200
geometrical stage time	12 min 36 s	12 min 36 s
post-processing time (reference)	47 min 38 s	15 min 58 s
post-processing time (cubic B-spline)	6 min 44 s	2 min 26 s
post-processing speedup	707%	656%
total simulation speedup	304%	190%
mean relative error (path gain)	0.39%	0.40%
mean relative error (rms delay spread)	0.67%	0.20%

doi: 10.1049/iet-map.2012.0306

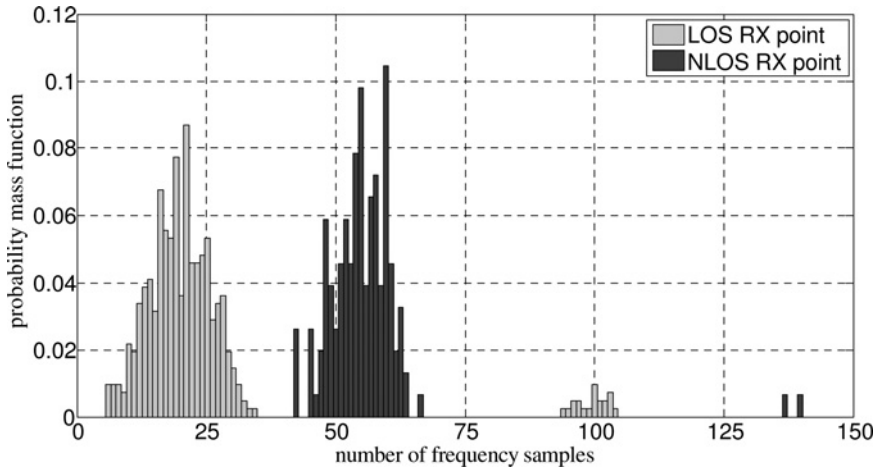

Fig. 9 *Probability mass function of the number of required frequency samples for cubic B-spline reconstruction of the multipath components' frequency response*

the number of required frequency samples for the arriving rays at a typical LOS point (along RX-line 1) and a typical NLOS point (along RX-line 2). The number of required frequency samples are concentrated in 10–25 range for the LOS point, whereas 50–65 frequency samples are usually required for reconstruction of the frequency responses of the rays that arrive at the NLOS point. The reason can be well understood by referring to the environment plan and the values of $\Delta f_R(\theta_i)$ and $\Delta f_T(\theta_i)$. According to the results of pre-processing, the value of $\Delta f_T(\theta_i)$ is in the range of 178–202 MHz for the brick wall that separates the two rooms. All rays that arrive at the NLOS point have been transmitted through this wall. As a result, the required frequency spacings for all these rays are inevitably less than 202 MHz. This means that at least 7.5 GHz/202 MHz $\simeq$ 38 samples are required in the NLOS case. Intersection with other walls and furniture further increases the number of samples and results in a curve shown in Fig. 9. In contrast, most rays that contribute in the LOS location are the resultant of multiple reflections by the objects inside the right-side room or transmissions through its cubicles. According to pre-processing and with reference to the average values of Δf_R and Δf_T in Table 1, we find that Δf_R (for walls, ceiling, floor and cubicles) and Δf_T (for cubicles) are relatively large. This results in less number of required samples.

The tails of the two graphs of Fig. 9 are associated with the rays that have passed through the central brick wall more than once. Some launched rays from the transmitter enter the left room and after some bounces return to the right room and illuminate the LOS receiver location. These rays have been transmitted through the central brick wall twice and are responsible for the tail of the LOS graph (around 100 samples). Similarly, the tail of the NLOS graph (around 140 samples) is related to those rays that have passed through the central brick wall three times before reaching the receiver. The cubic B-spline reconstruction of such rays is more computationally expensive but their population is much less than the total number of arriving rays at the RX points.

6 Conclusion

The utilisation of the cubic B-spline function in site-specific propagation modelling of UWB electromagnetic waves has been presented in this paper. The cubic B-spline function has a high accuracy and involves low-computational complexity when used as a reconstruction filter. By incorporating this function in the post-processing stage of ray tracing, the electromagnetic fields and the frequency response of the UWB channel can be reconstructed from a few frequency samples. Hence, a lot of unnecessary field calculations are avoided. The numerical results show that a speedup of several times can be achieved for a typical indoor environment.

A systematic procedure for selecting the necessary and sufficient number of frequency samples for cubic B-spline reconstruction of the frequency response has also been proposed. This procedure considers the frequency variations of transmitting and receiving antennas as well as the frequency dependence of the propagation mechanisms. Through an à priori simulation, the walls of the environment and the TX and RX antennas are labelled with descriptive functions. These functions are then incorporated in post-processing to find the number of the required frequency samples. The overall number of the frequency samples has been found to depend on the relative TX–RX position and on the site-specific nature of the environment.

7 References

1 Molisch, A.: 'Ultra-WideBand propagation channels', *Proc. IEEE*, 2009, **97**, (2), pp. 353–371
2 Molisch, A.: 'Ultrawideband propagation channels-theory, measurement, and modeling', *IEEE Trans. Veh. Technol.*, 2005, **54**, (5), pp. 1528–1545
3 Daniels, R., Heath, R.: '60 GHz wireless communications: emerging requirements and design recommendations', *IEEE Veh. Technol. Mag.*, 2005, **2**, (3), pp. 41–50
4 Ghavami, M.: 'Ultra wideband signals and systems in communication engineering' (Wiley, 2007, 2nd edn.)
5 Ghassemzadeh, S., Jana, R., Rice, C., Turin, W., Tarokh, V.: 'Measurement and modeling of an ultra-wide bandwidth indoor channel', *IEEE Trans. Commun.*, 2004, **52**, (10), pp. 1786–1796
6 Cassioli, D., Win, M., Molisch, A.: 'The ultra-wide bandwidth indoor channel: from statistical model to simulations', *IEEE J. Sel. Areas Commun.*, 2002, **20**, (6), pp. 1247–1257
7 Molisch, A., Cassioli, D., Chong, C.-C., *et al.*: 'A comprehensive standardized model for ultrawideband propagation channels', *IEEE Trans. Antennas Propag.*, 2006, **54**, (11), pp. 3151–3166
8 Malik, W., Edwards, D., Stevens, C.: 'Frequency dependence of fading statistics for ultrawideband systems', *IEEE Trans. Wirel. Commun.*, 2007, **6**, (3), pp. 800–804
9 Tiberi, G., Bertini, S., Monorchio, A., Giannetti, F., Manara, G.: 'Computationally efficient ray-tracing technique for modelling ultrawideband indoor propagation channels', *IET Microw. Antennas Propag.*, 2009, **3**, (3), pp. 395–401
10 Tiberi, G., Bertini, S., Malik, W., Monorchio, A., Edwards, D., Manara, G.: 'Analysis of realistic ultrawideband indoor communication channels

by using an efficient ray-tracing based method', *IEEE Trans. Antennas Propag.*, 2009, **57**, (3), pp. 777–785
11 Diskin, J., Brennan, C.: 'Accelerated ray-tracing for indoor ultra-wideband propagation modelling'. IEEE 65th Vehicular Technology Conf., April 2007, VTC2007-Spring, pp. 418–422
12 Burghelea, R., Avrillon, S., Uguen, B.: 'Efficient ray tracing post-processing schemes for UWB-IR channel simulation'. IEEE Antennas and Propagation Society Int. Symp., June 2009, APSURSI '09, pp. 1–4
13 Plouhinec, E., Uguen, B.: 'Ray-tracing and multiple reflections inside materials applied to UWB localization'. Int. Conf. Electromagnetics in Advanced Applications, September 2009, ICEAA '09, pp. 674–677
14 Mohtashami, V., Shishegar, A.A.: 'Accuracy and computational efficiency improvement of ray tracing using line search theory', *IET Microw. Antennas Propag.*, 2010, **4**, (9), pp. 1290–1299
15 Mohtashami, V., Shishegar, A.A.: 'Modified wavefront decomposition method for fast and accurate ray-tracing simulation', *IET Microw. Antennas Propag.*, 2012, **6**, (3), pp. 295–304
16 Suzuki, H., Mohan, A.: 'Ray tube tracing method for predicting indoor channel characteristics map', *Electron. Lett.*, 1997, **33**, (17), pp. 1495–1496
17 Barnes, P., Tesche, F.: 'On the direct calculation of a transient plane wave reflected from a finitely conducting half space', *IEEE Trans. Electromagn. Compat.*, 1991, **33**, (2), pp. 90–96
18 Pao, H.-Y., Dvorak, S., Dudley, D.: 'An accurate and efficient analysis for transient plane waves obliquely incident on a conductive half space (TE case)', *IEEE Trans. Antennas Propag.*, 1996, **44**, (7), pp. 918–924
19 Rothwell, E.: 'Efficient computation of the time-domain TM plane-wave reflection coefficient', *IEEE Trans. Antennas Propag.*, 2005, **53**, (10), pp. 3417–3419
20 Nai-Tong, Z., Jing, M.: 'Reflection characteristics analysis of IR-UWB signal'. Fourth Int. Conf. Wireless Communications, Networking and Mobile Computing, October 2008, WiCOM '08, pp. 1–4
21 Rothwell, E.J.: 'Plane-wave impulse response of a debye half space', *Electromagnetics*, 2008, **27**, (4), pp. 195–206
22 Saez de Adana, F., Gutiérrez, O., Navarro, M.A., Mohan, A.S.: 'Efficient time-domain ray-tracing technique for the analysis of ultra-wideband indoor environments including lossy materials and multiple effects', *Int. J. Antennas Propag.*, 2009, **2009**, pp. 1–8
23 Unser, M., Thevenaz, P., Aldroubi, A.: 'Shift-orthogonal wavelet bases using splines', *IEEE Signal Process. Lett.*, 1996, **3**, (3), pp. 85–88
24 Krumpholz, M., Katehi, L.P.B.: 'MRTD: new time-domain schemes based on multiresolution analysis', *IEEE Trans. Microw. Theory Tech.*, 1996, **44**, (4), pp. 555–571
25 Teixeira, F.L., Bergmann, J.R.: 'B-spline basis functions for moment-method analysis of axisymmetric reflector antennas', *Microw. Opt. Technol. Lett.*, 1997, **14**, (3), pp. 188–191
26 Hou, H., Andrews, H.: 'Cubic splines for image interpolation and digital filtering', *IEEE Trans. Acoust. Speech Signal Process.*, 1978, **26**, (6), pp. 508–517
27 Dahlquist, G., Bjorck, A.: 'Numerical methods in scientific computing: volume 1' (Society for Industrial Mathematics, 2008, Philadelphia, PA, USA)
28 Hamming, R.W.: 'Digital filters' (Dover Publications, 1997, 3rd edn.)
29 Unser, M., Aldroubi, A., Eden, M.: 'B-spline signal processing. I. theory', *IEEE Trans. Signal Process.*, 1993, **41**, (2), pp. 821–833
30 Balanis, C.A.: 'Advanced engineering electromagnetics' (Wiley, 1989)
31 Muqaibel, A., Safaai-Jazi, A., Bayram, A., Attiya, A., Riad, S.: 'Ultrawideband through-the-wall propagation'. IEE Proc. Microwaves, Antennas and Propagation, December 2005, pp. 581–588
32 Buehrer, R., Davis, W., Safaai-Jazi, A., Sweeney, D.: 'Ultra wideband propagation measurements and modeling – final report to DARPA NETEX Program'. Virginia Tech., Tech. Rep., 2004
33 Luebbers, R.: 'Finite conductivity uniform GTD versus knife edge diffraction in prediction of propagation path loss', *IEEE Trans. Antennas Propag.*, 1984, **32**, (1), pp. 70–76
34 Kouyoumjian, R., Pathak, P.: 'A uniform geometrical theory of diffraction for an edge in a perfectly conducting surface', *Proc. IEEE*, 1974, **62**, (11), pp. 1448–1461
35 McKown, J., Hamilton, R.L. Jr: 'Ray tracing as a design tool for radio networks', *IEEE Netw. Mag.*, 1991, **5**, (6), pp. 27–30
36 Seidel, S.Y., Rappaport, T.S.: 'Site-specific propagation prediction for wireless in-building personal communication system design', *IEEE Trans. Veh. Technol.*, 1994, **43**, (4), pp. 879–891
37 Torres, R.P., Valle, L., Domingo, M., Loredo, S.: 'An efficient ray-tracing method for radiopropagation based on the modified BSP algorithm'. IEEE VTS 50th Vehicular Technology Conf., Amsterdam, Netherlands, September 1999, VTC 1999 – Fall, vol. 4, pp. 1967–1971
38 Nagasawa, K., Matsuzuka, I.: 'Radiation field consideration of biconical horn antenna with different flare angles', *IEEE Trans. Antennas Propag.*, 1988, **36**, (9), pp. 1306–1310

doi: 10.1049/iet-map.2012.0306